Cell PRESS
Structure
Short Article

Cryo-Electron Microscopy Three-Dimensional Structure of the Jumbo Phage ΦRSL1 Infecting the Phytopathogen *Ralstonia solanacearum*

Grégory Effantin,[1] Ryosuke Hamasaki,[2] Takeru Kawasaki,[2] Maria Bacia,[3,4,5] Christine Moriscot,[1,3,4,5] Winfried Weissenhorn,[1] Takashi Yamada,[2,*] and Guy Schoehn[1,3,4,5,*]
[1]Unit of Virus Host-Cell Interactions, UMI 3265 UJF-EMBL-CNRS, 6 rue Jules Horowitz, 38042 Grenoble Cedex, France
[2]Department of Molecular Biotechnology, Graduate School of Advanced Sciences of Matter, Hiroshima University, Higashi-Hiroshima 739-8530, Japan
[3]CNRS
[4]CEA
[5]UJF-Grenoble-1
Institut de Biologie Structurale-Jean-Pierre Ebel, UMR 5075 41, rue Jules Horowitz, 38027 Grenoble Cedex, France
*Correspondence: tayamad@hiroshima-u.ac.jp (T.Y.), schoehn@embl.fr (G.S.)
http://dx.doi.org/10.1016/j.str.2012.12.017

SUMMARY

ϕRSL1 jumbo phage belongs to a new class of viruses within the *Myoviridae* family. Here, we report its three-dimensional structure determined by electron cryo microscopy. The icosahedral capsid, the tail helical portion, and the complete tail appendage were reconstructed separately to resolutions of 9 Å, 9 Å, and 28 Å, respectively. The head is rather complex and formed by at least five different proteins, whereas the major capsid proteins resemble those from HK97, despite low sequence conservation. The helical tail structure demonstrates its close relationship to T4 sheath proteins and provides evidence for an evolutionary link of the inner tail tube to the bacterial type VI secretion apparatus. Long fibers extend from the collar region, and their length is consistent with reaching the host cell surface upon tail contraction. Our structural analyses indicate that ϕRSL1 is an unusual member of the *Myoviridae* that employs conserved protein machines related to different phages and bacteria.

INTRODUCTION

Myoviridae phages represent about 25% of the *Caudovirales* (Ackermann, 2007) and use a contractile tail similar to a syringe to infect a broad range of bacteria (Browning et al., 2012). Among the *Myoviridae*, a new class of viruses carrying a large genome (over 200 kbp) has recently emerged, the "jumbo phages" (Hendrix, 2009), and tentatively classified into a seventh's myovirus genus, the "ϕKZ-like viruses genus" (Krylov et al., 2007). The prototype of this genus is the *Pseudomonas aeruginosa* phage ϕKZ (280 kbp; Mesyanzhinov et al., 2002), which is characterized by a large head, a contractile tail, and fibers surrounding the tail. The recently isolated lytic jumbo phage (ϕRSL1) carries a 240 kbp dsDNA genome, which is largely different from other phage genomes resembling only the *Pseudomonas putida* Lu11 phage genome (Adriaenssens et al., 2012). ϕRSL1 infects a wide panel of *Ralstonia solanacearum* strains (soil-borne Gram-negative bacterium) (Yamada et al., 2007).

SDS-PAGE analysis of the purified virus showed at least 25 structural proteins ranging from 13 to 160 kDa, which have none or low (<15%) primary sequence similarity to any known phage structural proteins (Yamada et al., 2010). Primary sequences of phage proteins are often highly divergent between different bacteriophages, but genomic, biochemical, and structural characterizations have revealed some unexpected relationships between them. For instance, despite differences in size and shape, their shells are all composed of one (or two) major capsid protein (MCP) having the same core fold as the *Siphoviridae* HK97 phage (Helgstrand et al., 2003). While the capsid's main building element is highly conserved, its stabilization mechanism is more variable and can be achieved through covalent crosslinking of the MCPs (Wikoff et al., 2000) or through interactions between peripheral domains encoded in the MCP itself (Morais et al., 2005). Other phages use additional external proteins to cement the MCPs together (Qin et al., 2010; Lander et al., 2008; Effantin et al., 2010).

Another unexpected evolutionary link has emerged between some phage tail proteins and the Gram-negative bacterial type VI secretion system (T6SS), which is implicated in various virulence-related processes (Leiman et al., 2009; Records, 2011). The secreted proteins of the Hcp and VgrG families are topologically related to several phage tail proteins including the tail tube proteins (Leiman et al., 2009).

Because it was speculated that ϕRSL1 could represent an evolutionary distinct branch of the *Myoviridae* family, we analyzed the three-dimensional (3D) structure of the entire ϕRSL1 by electron cryo microscopy (cryo-EM) to obtain insight into its evolutionary relationship with other phages. Each phage particle was split into head, helical shaft, and tail in order to reconstruct them independently and combine these substructures with a lower resolution model of the entire phage, highlighting the complexity of the jumbo phage. Our structural analyses reveal conserved features from HK97 and the type VI

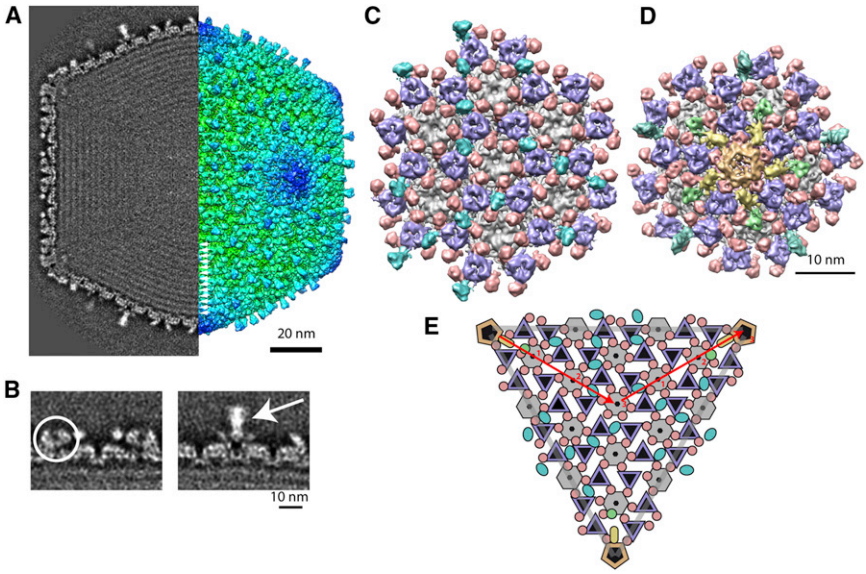

Figure 1. 3D Reconstruction of ϕRSL1 and Capsid Organization

(A) Central slice and isosurface representation of the 3D reconstruction at 9 Å resolution. The 13 concentric layers of DNA are visible (white arrows) in the left part, and the right part of the particle is colored according to its diameter (from green to dark blue).

(B) Zoomed views of the capsid density are shown for two decoration proteins: triskelion (left panel, circle) and spike (right panel, arrow).

(C) Close-up view around a segmented 3-fold axis of the ϕRSL1 head. The hexamers are colored in gray. Two types of decorating complexes can be recognized: a triskelion colored in pink and violet lying at the junction between three hexamers and a spike-like complex (cyan) bridging some pairs of triskelions.

(D) Close-up view of a segmented 5-fold axis of the ϕRSL1 head. The penton turret is colored in beige. Triskelions and spikes and colored like in (C), and the extra densities extending from the 5-fold axis are highlighted in yellow and green.

(E) Scheme of the ϕRSL1 capsid organization. One facet is represented, and the color code is the same as the one used in (C) and (D). The T = 27 symmetry is highlighted in red (h = 3; k = 3; $T = h^2 + k^2 + hk$).

See also Figure S1.

secretion apparatus, providing further evidence for structure-based elucidation of distant evolutionary relationships.

RESULTS

ϕRSL1 Head Structure

In a first step, only the phage capsid was selected from the cryo-EM images to perform icosahedral image analysis resulting in a 9 Å resolution 3D reconstruction (Figures 1A; Figure S1 available online). The diameter of the capsid (excluding the spikes) is 123 nm from vertex to vertex, 108 nm along the 2-fold symmetry axis, and follows a T = 27 triangulation symmetry with a planar outline (Figure 1E). The dimensions of the head match well with those of ϕKZ. Examination of the central slice of the 3D reconstruction of the head shows that the inner capsid layer is very thin (40 Å) and made by repetitive rectangular shaped densities separated by even thinner floor stretches (15 Å in thickness) (Figure 1B). An apparently discontinuous outer layer of protein is lying on top of this inner floor (Figure 1B, circle), and spikes are extending from the surface of the virus (Figure 1B, arrow). We also observed at least 13 concentric layers of DNA, each separated by ~22 Å (Figure 1A). Although such DNA packing is quite common in *Caudovirales* (Fokine et al., 2005; Effantin et al., 2006), the large layer number is in agreement with the large genome of ϕRSL1.

For each facet, the inner capsid layer (thinner part of the capsid plus rectangular densities) is built up by a lattice of hexamers and pentamers (Figures 1C–1E, gray). The shape and dimensions of the capsomers are similar to the one of the MCP of bacteriophage HK97 (Wikoff et al., 2000). The capsid contains 260 hexamers (13 per facet) and 11 pentamers (one vertex is occupied by the portal complex), which represent 1,615 copies of the MCP (Yamada et al., 2010). The X-ray structure (Protein Data Bank [PDB] ID: 1OHG) of HK97 (Helgstrand et al., 2003) fits snugly into ϕRSL1 despite the fact that there is nearly no sequence identity between their MCPs (14% over 360 residues; data not shown). The position of the 40 Å long α helix of the HK97 MCP matches very well with a long cylindrical rod visible in the ϕRSL1 EM map (Figures 2A and 2B, arrows); thus, this matching highlights another example of a dsDNA phage core capsid protein sharing the HK97 fold. However, there is no evidence that ϕRSL1 uses the same cross-linking stabilizing mechanism as HK97. Indeed, for HK97, some important residues for the covalent cross-linking are located on the E-loop, which doesn't fit well into ϕRSL1 EM density, and moreover, the catalytic triad is absent in the ϕRSL1 sequence. Therefore, ϕRSL1 capsid stabilization may be achieved by a different mechanism.

ϕRSL1 displays a complex set of outer additional proteins, some of which may contribute to capsid stabilization (Figures 1 and 2). They can be classified into vertex- (Figures 1D and 2A) and facet-decorating (Figures 1C, 2C, and 2D) groups. For the vertices, an additional protein is covering the penton. Although the X-ray structure of the HK97 MCP fits into the major part of the EM density map, a large outer crown of density is left empty (Figures 1D and 2A, beige). This density solely interacts with the tip of the penton and with the pink part of the peripentonal triskelion (see below) but not with the inner layer of the capsid. Therefore, it does not contribute directly to its stabilization. A second group of additional proteins is expanding radially from the penton toward the hexamers (Figures 1D and 1E, yellow and green) and is most likely composed of two proteins. They make direct contact with the inner layer of the capsid at both the penton/hexamer interface (yellow) and the peripentonal hexamers (green). The closest protein from the vertex (Figure 1D, yellow) also contacts the penton cap. We suggest

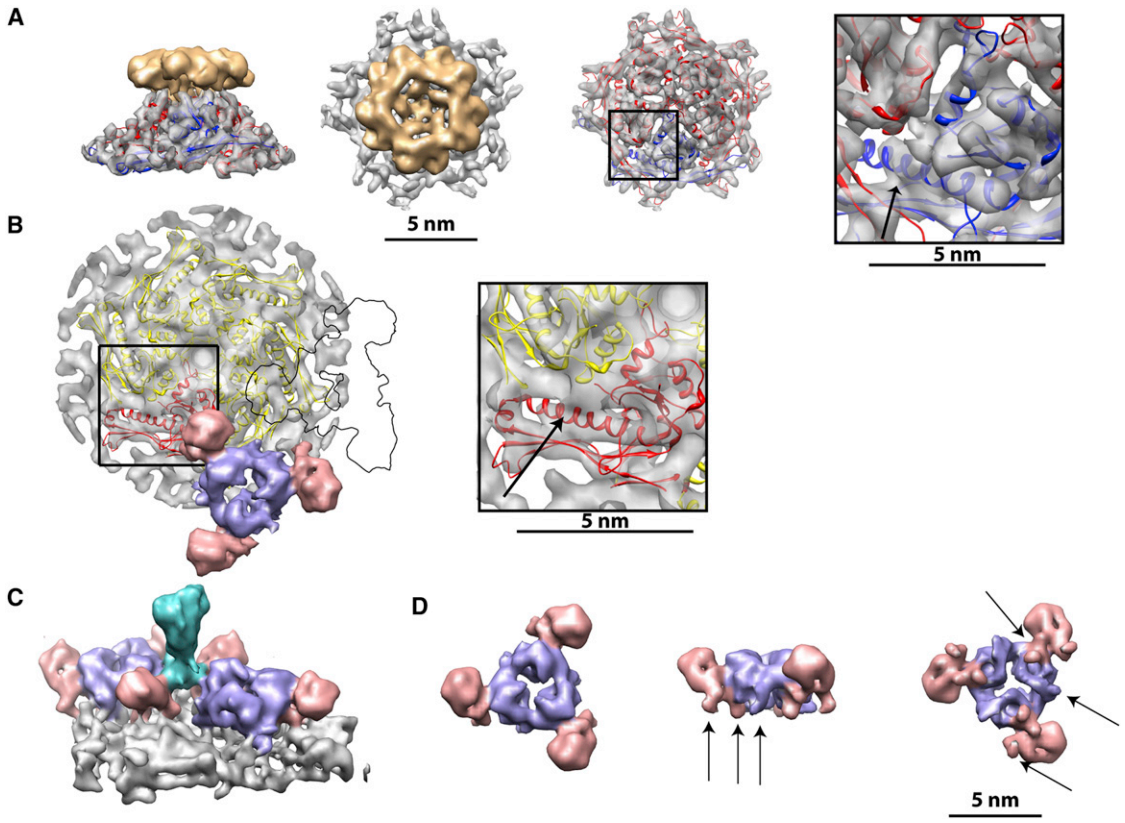

Figure 2. Dissection of ϕRSL1 Capsid Organization

(A) Detailed view of a segmented penton. The penton can be split into a lower part (gray color), which is similar to HK97 MCP and an upper part (beige color). There is a small connection between the two parts. The docked HK97 MCP X-ray structure (PDB ID: 1OHG) is represented as a red ribbon with the exception of one blue monomer; the arrow highlights the 40 Å long α helix of HK97.

(B) Fitting of the HK97 MCP X-ray structure into ϕRSL1 hexamer density; the 40 Å long α helix is clearly visible (arrow). HK97 hexamer is represented as yellow ribbons, with the exception of one red monomer. One 3D triskelion as well as the contour of a second one has been added to highlight the triskelion footprint on the hexamer.

(C) Detailed side view of the triskelions-spike interaction. The spike (cyan) only contacts the two triskelions (violet and pink) and not the capsid floor (gray).

(D) Triskelion trimer (core in violet, globular extension in pink) seen in three different orientations (top, side, and bottom from left to right, respectively). The arrows highlight the small rod-like densities making the contact with the MCP.

Some areas have been magnified ×2 for clarity (squares and rectangle). See also Figures S1 and S2.

that these peripentonal proteins aid in capsid stabilization at the vertices.

For the facet, triskelion-shaped structures are located at all local and strict 3-fold axes on top of the MCP layer, following the same T = 27 geometry (Figures 1B, 1C, and 1E, violet and pink). Each triskelion is made of a central triangular body plus a globular extra density attached to each of the three body vertices (Figures 2B and 2D). There are 27 trimeric triskelions present on each facet (1,620 monomers in total), covering the entire surface of the head. Thus, this complex is almost as abundant in the virus as the MCP. According to the SDS-PAGE gel and mass spectrometry assignment (Figure S2), the most intense band corresponds to ORF136 (33 kDa) which was shown to be the MCP (Yamada et al., 2010). The second most prominent band corresponds to ORF135 and has a molecular weight of 24.7 kDa. Estimation of the entire triskelion volume from our map suggests that this density could accommodate at least 60 kDa. The triskelion is therefore probably a trimer of a two domain protein. Connections to the inner floor are made via three different 10 Å diameter cylinders, two deriving from the external globular part of the triskelion and one from the triangular part (Figures 2B and 2D).

The last decorating density is a 60 Å tall spike-like smooth density extending from the head surface. It is present in between some of the triskelion pairs (15 per facet) and has a flared shape (Figures 1A, 1E, and 2C, cyan). This complex is probably a homodimer according to its shape and by its position on a non-imposed local 2-fold symmetry axis. Only 15 out of 32 potential binding sites per facet are occupied due to geometrical constraints; the center-to-center distance between two triskelions carrying a spike is 5 Å smaller compared to the one where the spike is absent (Figures S1C and S1D).

The Helical Tail Structure

The contractile tail of ϕRSL1 is 105 nm long (from the collar to the end of the puncturing apparatus) in its extended conformation. The helical part is 72 nm in length and 24.5 nm in diameter (Figures 3A, 4A, S1A, and S4B). Like other phages,

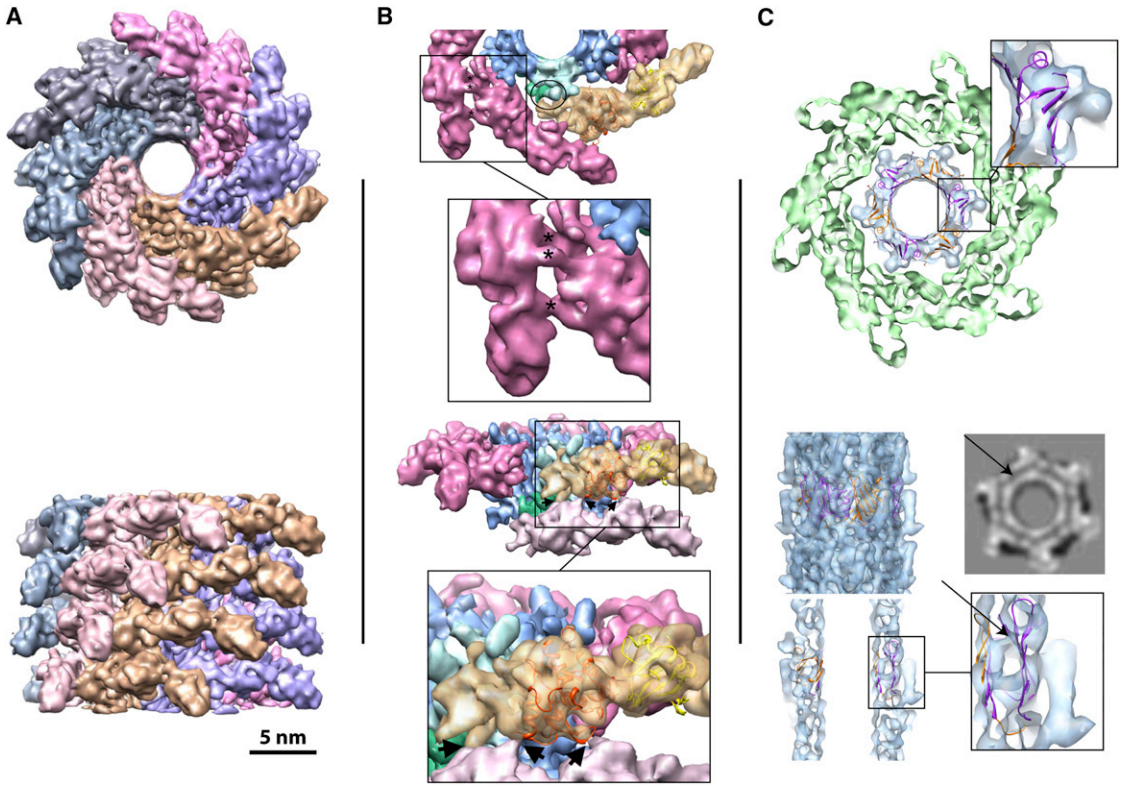

Figure 3. The ϕRSL1-Helical Tail

(A) 3D structure of the 9 Å-helical shaft seen in the top view (top image) and side view orientations (bottom). Each of the six-helical strands is colored differently.

(B) Fitting of T4 tail sheath X-ray structure (PDB ID: 3FOA) into the ϕRSL1 EM density (upper image, top view; lower image, side view). One ϕRSL1 tail sheath monomer is shown in transparent orange, while the other monomers are colored in pink. The docked T4 domains II and III are represented by ribbons in yellow and light red, respectively. The tail tube is colored in blue. Contacts between the tube and the sheath proteins are highlighted (circle) as well as contacts between the two sheath monomers from two successive rings (arrows, bottom panel) or from the same ring (upper panel, asterisks). In the bottom panel, one (pink) sheath monomer from the upper ring was removed to allow the visualization of the ring-ring interaction (arrows).

(C) Fitting of T6SS protein (PDB ID: 3EEA) into the inner tube cryo-EM density. Top panel: Thin slab through the ϕRSL1 tail reconstruction [top view as in (A), top image]. The sheath density is colored in light green, while the inner tube is colored in transparent blue, with the docked T6SS hexamer shown in ribbon diagram (with alternating monomers in orange and magenta). The arrow in the enlarged rectangular box indicates the only α helix of the T6SS protein fitting into a rod-like density of the EM map. Bottom panels: Side view of the inner tube docking. The upper left image is a front view. The lower left image (and the corresponding enlarged view on the right) is a thin central slab through the tube and shows two parallel walls of density, making the inner tube separated by a lower density (arrow). The two walls are also visible as two concentric rings of density in the upper right grayscale section of the tube (top view orientation). Some areas have been magnified ×2 for clarity (squares and rectangle).

See also Figures S1 and S3.

the contractile tail sheath of ϕRSL1 is assembled around the tail tube. Both are following the same helical symmetry with an additional 6-fold symmetry around the tail axis and are composed of 19 hexameric rings (114 copies of the monomer in total). Each ring is separated by 37.9 Å, and the rotation between one ring monomer and the next is 22.1° (Figure 3A). An overall comparison of the T4 and ϕRSL1-helical tail assembly clearly highlights their relationship. The T4 tail sheath protein contains four domains (I–IV), and 75% of its structure has been solved by X-ray crystallography (domains I–III) (Figures S3C and S3D) (Aksyuk et al., 2009). Domains II and III constitute most of the body of the protein, while domain I and the C-terminal domain IV (which structure is unknown) point toward the exterior and the interior of the tail, respectively. Sequence alignment between T4 and the ϕRSL1 tail sheath proteins shows weak but significant homologies; domains III and IV exhibit a higher degree of homology than domains I and II (Figures S3A and S3B). Because of the similar molecular weights of the T4 (Aksyuk et al., 2009) and ϕRSL1 sheath proteins (71 kDa and 65 kDa, respectively), domains II and III could reliably fit separately into the ϕRSL1 map (Figure 3B). T4 domain I has a similar size as the corresponding ϕRSL1 domain (Figures 3B and S3D) and could be fit into the EM density. However, the docking is not unambiguous, and its position in ϕRSL1 is largely different from T4 (Figure S3E). The subnanometric view of the ϕRSL1 tail we obtained is, to our knowledge, the best resolution achieved to date for a bacteriophage tail by cryo-EM (Figure 3A) and allows the visualization of the contacts between the sheath and the tube as well as the one between sheath proteins from the same ring or from two successive rings (three main contacts for each; Figure 3B, stars and small arrows). The T4 tail sheath docking of domains II and III indicates that most of the tail sheath interactions involve

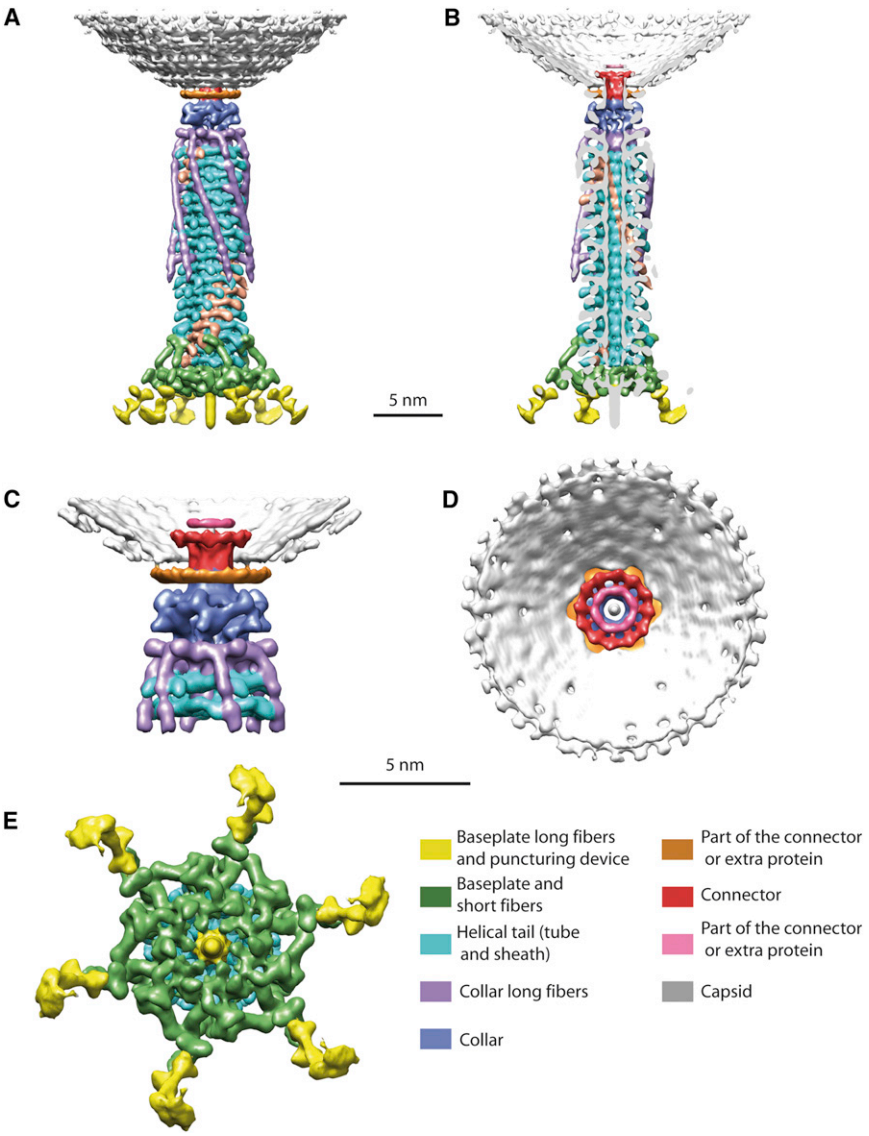

Figure 4. Entire Tail 3D Reconstruction
(A–E) 3D reconstruction of the entire tail at 28Å resolution. (A) Front view of the tail. (B) Same as in (A) with the front half removed to reveal the interior. (C) Detailed side view of the connector. (D) Detailed top view of the connector seen from the inside of the capsid. (E) Magnified view of the baseplate (seen from the bottom).
The different colors are labeled. See also Figures S1 and S4.

domains II, III, and IV. The ϕRSL1 domain I equivalent (the most exterior density) is marginally contributing to the observed interactions. The tail inner tube forms a barrel-like structure with a nearly continuous flat surface on the inside (Figure 3C). The outside surface is almost as flat, with the exception of small (40 Å in height, 10 Å in width) protruding, rod-like densities (Figures 3B, oval, and 3C) lying parallel to the tube wall and making contacts with the outer tail sheath while bridging two tail tube monomers of two consecutive rings. The ϕRSL1 tail tube protein (169 amino acids) showed limited sequence similarities to other phage tail tube proteins, including T4 gp19 (25% identity over 130 residues). Using a structure/prediction server (http://meta.bioinfo.pl; Ginalski et al., 2003), weak hits with the T6SS family including EvpC from *Edwardsiella tarda* (PDB ID: 3EAA) and Hcp3 (PDB ID: 3HE1) (Jobichen et al., 2010; Osipiuk et al., 2011) from *Pseudonomas aeruginosa* have been found (data not shown). The T4 tail tube protein was also proposed to be structurally similar to Hcp1 (Leiman et al., 2009), which is consistent with the predicted homology between Hcp-like proteins and the ϕRSL1 tail tube. The core region of the Hcp-like monomer is composed of antiparallel β strands assembling in two β sheets, forming a β barrel of 12 Å diameter with an additional α helix on one side. These proteins assemble as hexamers with a 40 Å hole, and their interior wall is solely made of β strands. Ab initio secondary structure prediction of ϕRSL1 tail tube protein by psipred (McGuffin et al., 2000; Buchan et al., 2010) also showed a protein composed of β strands with one α-helical region in the middle of the sequence (data not shown). When docked into the cryo-EM inner tube density, the dimensions of the Hcp-like ring (PDB ID: 3EAA) are remarkably similar (Figure 3C). Furthermore, the antiparallel β barrel fold fits the EM density nicely, and the gap at the center of the β barrel separating the two β sheets is clearly visible (Figure 3C, bottom panel, arrows). The additional α helix (adjacent to the β barrel and conserved in Hcp-like proteins) also fits into one of the rod-like densitities of the EM map (Figure 3C, top panel, arrow). Despite their low sequence homology, our results suggest that the ϕRSL1 tail tube is topologically and structurally related to T6SS proteins. It should be noted that the rod-like densities described above (Figure 3B, oval), linking the tail tube to the tail sheath, are not modeled by the T6SS docking (Figure 3C), while the Hcp-like and ϕRSL1 tail tube monomers are almost the same size (163 and 169 residues respectively). The rods, therefore, belong to the C-terminal part of the tail sheath or to a different protein and are probably involved in the sliding of the sheath protein relative to the inner tube during tail contraction.

Full Tail Structure

Several other complexes are associated with the sheath-inner tube complex: connector, baseplate, fibers, etc. All the tails that were entirely visible in the micrographs have been isolated in silico and subjected to single particle image analysis, imposing only 6-fold symmetry along the tail axis (Figures 4A and 4B). The obtained structure is of lower resolution because of the smaller

data set (approximately 28 Å; Figure S1). The baseplate and connector regions were isolated from the entire tail data set and further refined to 21 and 22.5 Å, respectively (Figures 4C, 4D, 4E, and 1B). Despite the limited resolution obtained, it is possible to distinguish the different components of the tail going from the head to the tail extremity. The connector (red in Figures 4C and 4D) exhibits a common 12-fold symmetry although only a 6–fold symmetry was imposed. Immediately below are the collar components (orange and dark blue), which anchor six long fibers (Figure 4, purple). They are wrapped tightly around the upper helical portion (the first 11 rings) of the tail (Figure 4, turquoise) by interacting directly with the tip of the tail sheath monomers (domain I) of every two rings. The baseplate components start to interact with the tail sheath in the last four rings of the helical portion of the tail. There is not enough information on the multiple components of the baseplate for ϕRSL1 to identify them in the EM map at the present resolution. Only the tip, which acts as a puncturing device, and the beginning of the long tail fibers has been segmented out (Figure 4, yellow).

DISCUSSION

For comparison with ϕRSL1, another jumbo phage, ϕKZ, has a capsid of slightly bigger dimensions with the same triangulation number but a larger MCP that includes an extra domain stabilizing the capsid at each 2-fold axis (Fokine et al., 2005). In contrast, HK97 has a coat protein of the same size as ϕRSL1 and much smaller capsid dimensions (660 Å maximum diameter), and stabilization is achieved by covalent cross-linking between subunits. For ϕRSL1, a different configuration prevails with large capsid dimensions, a small coat protein size without cross-linking capabilities. This may explain why ϕRSL1 has an extra layer of protein linking all the capsomers together and forming an almost complete cage-like assembly on its surface: the triskelions. The cage is completed by radial peripentonal density (Figure 1, yellow and green), cementing penton and peripentonal hexamer together. Thus, these additional proteins are probably present to reinforce particle stability. The local 3-fold stabilization achieved by the triskelions is a common feature of phages (Soc trimers for T4 [Qin et al., 2010], GpD trimers for lambda [Lander et al., 2008], extra domain of the MCP for CW02 [Shen et al., 2012], or GpD-like complexes for Gifsy-2 [Effantin et al., 2010]). Indeed, the central triangular body of ϕRSL1 triskelions resembles the lambda GpD trimers (although no fit is possible) but without the long α-helical extension interacting with the coat protein (Lander et al., 2008). As judged by the complexity of the ϕRSL1 capsid compared to smaller phages, a general rule can be deduced: larger phages may more systematically require several additional proteins besides their MCPs to ensure correct capsid assembly and a more robust stabilization mechanism. The architectural uniqueness of ϕRSL1 particles may explain its remarkable stability at higher temperatures (37°C–50°C) in natural environments (Fujiwara et al., 2011).

A second type of decoration protein extends from the capsid, and this protein is either located on top of the penton, forming a turret-like structure, or on the capsid facet in the form of a spike-like structure. Their locations and shapes as well as a tentative interpretation of the penton turrets as immunoglobulin domains (Lander et al., 2012) suggest that they could play a role in recognition events as reported for T4 and SIO-2 (Fokine et al., 2011; Lander et al., 2012). The ϕRSL1 protruding spikes, as described for SPP1 (White et al., 2012), can serve as an anchor to attach to different surfaces, allowing the phage to be transported until it finds a bacterium to infect. ϕRSL1 is almost completely covered by potential ''sensing'' and anchor proteins.

The ϕRSL1 tail is topologically quite similar to other known *Myoviridae* tails and can be schematically decomposed into three regions: the collar, the helical tail, and the baseplate. For the helical tail, the axial rise and azimuthal angle between subunits are in close agreement with other phages: 37.9 Å/22.1°; 40.6 Å/17.2°, and 36.2 Å/22° for ϕRSL1, T4 (Kostyuchenko et al., 2005), and ϕKZ (Fokine et al., 2007), respectively. This implies that the tail sheath fold for the contractile tails should be well conserved between these phages as well. The convincing fit of the inner domains of the T4 sheath protein (involved in inter- and intra-sheath protein contacts) into the corresponding ϕRSL1 densities confirms this. In contrast, the less conserved external part of the sheath protein, which interacts with the long fibers and the baseplate proteins, is logically more divergent, at least between ϕRSL1 and T4.

An intriguing part of the tail is the presence of long fibers starting from the collar. The recording of a few images of the contracted state of the tail (Figure S4) reveals that the long collar fibers, which were lying along the tail, are now not only detached, but the shorter contracted tail enables the fibers to be in direct contact with the cell surface (i.e., their end is at the same level as the baseplate; Figure S4A, arrow). We hypothesize that once the tail is contracted, the long collar fibers can efficiently anchor the phage to the host cell surface. Extra host cell anchoring mechanisms may be especially useful for jumbo phages as injection of their large genome may take longer than for smaller phages.

Finally, based on bioinformatics prediction and fitting data, we also propose that the ϕRSL1 tail tube protein has a similar fold as T6SS-related proteins. Our finding adds to the accumulating evidences that components of bacteriophage tail and bacterial secretion systems share a common origin and that distant relationships between proteins of different functions can be revealed through their structural comparison.

As more structures of bacteriophages become available, the most conserved domains of key proteins of the capsid and tail are emerging. They can be seen as the elementary building blocks that link all phages together. However, extra domains of these elementary blocks as well as the remaining decorating proteins exhibit greater variability. ϕRSL1, for instance, has developed two additional types of decoration proteins, which are most likely involved in capsid stabilization or cell recognition and attachment. Once ϕRSL1 has found a host, the long fibers might help in maintaining the phage in place until the entire DNA has been injected. In summary, ϕRSL1 is a jumbo phage exhibiting a very high degree of complexity. Additional future information on the phage composition will allow further detailed analysis of its structure.

EXPERIMENTAL PROCEDURES

See the Supplemental Experimental Procedures for a more detailed explanation.

Electron Microscopy

Negative Staining

The phages have been stained using 2% ammonium molybdate pH 7.5 and imaged in a CM12 Philips EM using an Orius SC1000 CCD camera.

Cryo-EM

The vitrified samples have been imaged in a Polara EM (FEI) working at 300kV on KODAK SO-163 films.

Image Analysis

Phage Head Reconstruction

Phage head images have been analyzed with the model-based PFT2/EM3DR2 package (Fuller et al., 1996). 4,520 particles out of 6,232 were used for the final reconstruction.

ϕRSL1 Helical Tail Reconstruction

Phage tails were picked in consecutive overlapping segments (11,146) and reconstructed using custom scripts embedding the iterative helical real space reconstruction (IHRSR) method (Egelman, 2010). An extra 6-fold symmetry was imposed during the refinement. The IHRSR helical parameter search converged repeatedly to an axial rise z = 37.87 Å and an angle per subunit $\phi = 22.1^{\circ}$. The final 3D reconstruction includes 8,452 segments.

3D Reconstruction of ϕRSL1 Full Tail

Full tails images were subjected to projection matching image analysis imposing only 6-fold symmetry. Included in the final reconstruction were 1,153 out of 1,463 images.

Docking and Segmentation

The different fittings were done with CHIMERA (Pettersen et al., 2004) and the SITUS package (Wriggers et al., 1999).

ACCESSION NUMBERS

The EM maps were uploaded into the EM database associated with the Macromolecular Structure Database under the accession numbers EMD-2243, EMD-2244, EMD-2245, EMD-2246, and EMD-2247.

SUPPLEMENTAL INFORMATION

Supplemental Information includes four figures and Supplemental Experimental Procedures and can be found with this article online at http://dx.doi.org/10.1016/j.str.2012.12.017.

ACKNOWLEDGMENTS

We thank Daphna Fenel for excellent technical assistance. This work was partially supported by the Agence Nationale de la Recherche (ANR-08-BLAN-0271-01 to W.W. and G.S.), the Région Rhône-Alpes (to G.S.), and the GRAL labex grant (to C.M.). G.E. is supported by a postdoctoral fellowship from the Agence Nationale de Recherche sur le Sida (ANRS). The Polara microscope is part of the IBS Structural Biology and Dynamics GIS-IBISA-labeled platform.

Received: October 15, 2012
Revised: December 4, 2012
Accepted: December 18, 2012
Published: February 5, 2013

REFERENCES

Ackermann, H.W. (2007). 5500 Phages examined in the electron microscope. Arch. Virol. *152*, 227–243.

Adriaenssens, E.M., Mattheus, W., Cornelissen, A., Shaburova, O., Krylov, V.N., Kropinski, A.M., and Lavigne, R. (2012). Complete genome sequence of the giant Pseudomonas phage Lu11. J. Virol. *86*, 6369–6370.

Aksyuk, A.A., Leiman, P.G., Kurochkina, L.P., Shneider, M.M., Kostyuchenko, V.A., Mesyanzhinov, V.V., and Rossmann, M.G. (2009). The tail sheath structure of bacteriophage T4: a molecular machine for infecting bacteria. EMBO J. *28*, 821–829.

Browning, C., Shneider, M.M., Bowman, V.D., Schwarzer, D., and Leiman, P.G. (2012). Phage pierces the host cell membrane with the iron-loaded spike. Structure *20*, 326–339.

Buchan, D.W.A., Ward, S.M., Lobley, A.E., Nugent, T.C.O., Bryson, K., and Jones, D.T. (2010). Protein annotation and modelling servers at University College London. Nucleic Acids Res. *38*(Web Server issue), W563–W568.

Effantin, G., Boulanger, P., Neumann, E., Letellier, L., and Conway, J.F. (2006). Bacteriophage T5 structure reveals similarities with HK97 and T4 suggesting evolutionary relationships. J. Mol. Biol. *361*, 993–1002.

Effantin, G., Figueroa-Bossi, N., Schoehn, G., Bossi, L., and Conway, J.F. (2010). The tripartite capsid gene of Salmonella phage Gifsy-2 yields a capsid assembly pathway engaging features from HK97 and lambda. Virology *402*, 355–365.

Egelman, E.H. (2010). Reconstruction of helical filaments and tubes. Methods Enzymol. *482*, 167–183.

Fujiwara, A., Fujisawa, M., Hamasaki, R., Kawasaki, T., Fujie, M., and Yamada, T. (2011). Biocontrol of *Ralstonia solanacearum* by treatment with lytic bacteriophages. Appl. Environ. Microbiol. *77*, 4155–4162.

Fokine, A., Kostyuchenko, V.A., Efimov, A.V., Kurochkina, L.P., Sykilinda, N.N., Robben, J., Volckaert, G., Hoenger, A., Chipman, P.R., Battisti, A.J., et al. (2005). A three-dimensional cryo-electron microscopy structure of the bacteriophage phiKZ head. J. Mol. Biol. *352*, 117–124.

Fokine, A., Battisti, A.J., Bowman, V.D., Efimov, A.V., Kurochkina, L.P., Chipman, P.R., Mesyanzhinov, V.V., and Rossmann, M.G. (2007). Cryo-EM study of the Pseudomonas bacteriophage phiKZ. Structure *15*, 1099–1104.

Fokine, A., Islam, M.Z., Zhang, Z., Bowman, V.D., Rao, V.B., and Rossmann, M.G. (2011). Structure of the three N-terminal immunoglobulin domains of the highly immunogenic outer capsid protein from a T4-like bacteriophage. J. Virol. *85*, 8141–8148.

Fuller, S.D., Butcher, S.J., Cheng, R.H., and Baker, T.S. (1996). Three-dimensional reconstruction of icosahedral particles—the uncommon line. J. Struct. Biol. *116*, 48–55.

Ginalski, K., Elofsson, A., Fischer, D., and Rychlewski, L. (2003). 3D-Jury: a simple approach to improve protein structure predictions. Bioinformatics *19*, 1015–1018.

Helgstrand, C., Wikoff, W.R., Duda, R.L., Hendrix, R.W., Johnson, J.E., and Liljas, L. (2003). The refined structure of a protein catenane: the HK97 bacteriophage capsid at 3.44 A resolution. J. Mol. Biol. *334*, 885–899.

Hendrix, R.W. (2009). Jumbo bacteriophages. Curr. Top. Microbiol. Immunol. *328*, 229–240.

Jobichen, C., Chakraborty, S., Li, M., Zheng, J., Joseph, L., Mok, Y.K., Leung, K.Y., and Sivaraman, J. (2010). Structural basis for the secretion of EvpC: a key type VI secretion system protein from Edwardsiella tarda. PLoS ONE *5*, e12910.

Kostyuchenko, V.A., Chipman, P.R., Leiman, P.G., Arisaka, F., Mesyanzhinov, V.V., and Rossmann, M.G. (2005). The tail structure of bacteriophage T4 and its mechanism of contraction. Nat. Struct. Mol. Biol. *12*, 810–813.

Krylov, V.N., Dela Cruz, D.M., Hertveldt, K., and Ackermann, H.W. (2007). ''phiKZ-like viruses'', a proposed new genus of myovirus bacteriophages. Arch. Virol. *152*, 1955–1959.

Lander, G.C., Evilevitch, A., Jeembaeva, M., Potter, C.S., Carragher, B., and Johnson, J.E. (2008). Bacteriophage lambda stabilization by auxiliary protein gpD: timing, location, and mechanism of attachment determined by cryo-EM. Structure *16*, 1399–1406.

Lander, G.C., Baudoux, A.C., Azam, F., Potter, C.S., Carragher, B., and Johnson, J.E. (2012). Capsomer dynamics and stabilization in the T = 12 marine bacteriophage SIO-2 and its procapsid studied by CryoEM. Structure *20*, 498–503.

Leiman, P.G., Basler, M., Ramagopal, U.A., Bonanno, J.B., Sauder, J.M., Pukatzki, S., Burley, S.K., Almo, S.C., and Mekalanos, J.J. (2009). Type VI secretion apparatus and phage tail-associated protein complexes share a common evolutionary origin. Proc. Natl. Acad. Sci. USA *106*, 4154–4159.

McGuffin, L.J., Bryson, K., and Jones, D.T. (2000). The PSIPRED protein structure prediction server. Bioinformatics *16*, 404–405.

Mesyanzhinov, V.V., Robben, J., Grymonprez, B., Kostyuchenko, V.A., Bourkaltseva, M.V., Sykilinda, N.N., Krylov, V.N., and Volckaert, G. (2002). The genome of bacteriophage phiKZ of Pseudomonas aeruginosa. J. Mol. Biol. *317*, 1–19.

Morais, M.C., Choi, K.H., Koti, J.S., Chipman, P.R., Anderson, D.L., and Rossmann, M.G. (2005). Conservation of the capsid structure in tailed dsDNA bacteriophages: the pseudoatomic structure of φ29. Mol. Cell *18*, 149–159.

Osipiuk, J., Xu, X., Cui, H., Savchenko, A., Edwards, A., and Joachimiak, A. (2011). Crystal structure of secretory protein Hcp3 from Pseudomonas aeruginosa. J. Struct. Funct. Genomics *12*, 21–26.

Pettersen, E.F., Goddard, T.D., Huang, C.C., Couch, G.S., Greenblatt, D.M., Meng, E.C., and Ferrin, T.E. (2004). UCSF Chimera—a visualization system for exploratory research and analysis. J. Comput. Chem. *25*, 1605–1612.

Qin, L., Fokine, A., O'Donnell, E., Rao, V.B., and Rossmann, M.G. (2010). Structure of the small outer capsid protein, Soc: a clamp for stabilizing capsids of T4-like phages. J. Mol. Biol. *395*, 728–741.

Records, A.R. (2011). The type VI secretion system: a multipurpose delivery system with a phage-like machinery. Mol. Plant Microbe Interact. *24*, 751–757.

Shen, P.S., Domek, M.J., Sanz-García, E., Makaju, A., Taylor, R.M., Hoggan, R., Culumber, M.D., Oberg, C.J., Breakwell, D.P., Prince, J.T., and Belnap, D.M. (2012). Sequence and structural characterization of great salt lake bacteriophage CW02, a member of the T7-like supergroup. J. Virol. *86*, 7907–7917.

Wikoff, W.R., Liljas, L., Duda, R.L., Tsuruta, H., Hendrix, R.W., and Johnson, J.E. (2000). Topologically linked protein rings in the bacteriophage HK97 capsid. Science *289*, 2129–2133.

White, H.E., Sherman, M.B., Brasilès, S., Jacquet, E., Seavers, P., Tavares, P., and Orlova, E.V. (2012). Capsid structure and its stability at the late stages of bacteriophage SPP1 assembly. J. Virol. *86*, 6768–6777.

Wriggers, W., Milligan, R.A., and McCammon, J.A. (1999). Situs: A package for docking crystal structures into low-resolution maps from electron microscopy. J. Struct. Biol. *125*, 185–195.

Yamada, T., Kawasaki, T., Nagata, S., Fujiwara, A., Usami, S., and Fujie, M. (2007). New bacteriophages that infect the phytopathogen *Ralstonia solanacearum*. Microbiology *153*, 2630–2639.

Yamada, T., Satoh, S., Ishikawa, H., Fujiwara, A., Kawasaki, T., Fujie, M., and Ogata, H. (2010). A jumbo phage infecting the phytopathogen *Ralstonia solanacearum* defines a new lineage of the Myoviridae family. Virology *398*, 135–147.